Article

Estimation of State of Charge of Lithium-Ion Batteries Used in HEV Using Robust Extended Kalman Filtering

Caiping Zhang [1,*], Jiuchun Jiang [1], Weige Zhang [1] and Suleiman M. Sharkh [2]

[1] School of Electrical Engineering, Beijing Jiaotong University, Beijing 100044, China;
E-Mails: jcjiang@bjtu.edu.cn (J.J.); wgzhang@bjtu.edu.cn (W.Z.)

[2] School of Engineering Sciences, University of Southampton, Highfield, Southampton SO17 1BJ, UK;
E-Mail: S.M.Abu-Sharkh@soton.ac.uk

* Author to whom correspondence should be addressed; E-Mail: cpzhang@bjtu.edu.cn;
Tel.: +86-10-5168-3907; Fax: +86-10-5168-3907.

Abstract: A robust extended Kalman filter (EKF) is proposed as a method for estimation of the state of charge (SOC) of lithium-ion batteries used in hybrid electric vehicles (HEVs). An equivalent circuit model of the battery, including its electromotive force (EMF) hysteresis characteristics and polarization characteristics is used. The effect of the robust EKF gain coefficient on SOC estimation is analyzed, and an optimized gain coefficient is determined to restrain battery terminal voltage from fluctuating. Experimental and simulation results are presented. SOC estimates using the standard EKF are compared with the proposed robust EKF algorithm to demonstrate the accuracy and precision of the latter for SOC estimation.

Keywords: lithium-ion batteries; SOC estimation; robust estimation; EKF; HEV

1. Introduction

Lithium-ion batteries have become a promising alternative power source in electric vehicles (EVs) and power assist units used in hybrid electric vehicles (HEVs). Their advantages include high nominal cell voltage, high energy density, long life and not having a memory effect. As one of the power supplies on a vehicle, the performance of lithium-ion batteries will have direct impact on the driving performance of the vehicle. It is necessary for the battery to be effectively managed to improve its

performance and extend its lifetime. The main components of a battery management system include state of charge (SOC) estimation, cell balancing, thermal management, and safety control. The SOC, which describes the percentage of the battery available capacity to its rated capacity, is a key parameter in the battery management system. Accurate estimation of the SOC of the battery is also important for accurate simulation and optimization, and real time energy management of HEVs and EVs.

Techniques for estimation of the SOC of a battery may be categorized as direct computational methods or intelligent computational methods. Direct computational methods calculate the SOC of the battery directly based on its relationship with measurable battery parameters, for example, using ampere hour counting, open-circuit voltage, or internal impedance [1–3]. These methods are extensively used in HEV and EV applications since they are easy to implement. However, they suffer from relatively poor accuracy due to accumulative errors [4], especially when ampere hour counting is used.

Intelligent computational methods include those using artificial neural networks and extended Kalman filtering. The artificial neural networks approach has the advantage of adaptive learning, and can cope with the battery's nonlinear characteristics during charging and discharging. It has been investigated and used by many researchers [5,6]. However, the algorithm requires a large amount of data for training, and the accuracy of these models is affected significantly by the training data and training method.

In the extended Kalman filtering (EKF) approach the battery is regarded as a dynamic system, and the SOC is considered as an internal state of the dynamic system. Optimal state estimates can be obtained by adjusting the filter gain [7]. Using EKF to estimate the SOC of batteries has been the subject of extensive study in recent years due to its high accuracy and suitability for real time implementation [8–11]. For an accurate estimate of the SOC, the EKF requires accurate system modeling as well as knowledge of the statistical properties of the system noise. However, in practice, the dynamic system model and the covariance matrices cannot be precisely determined especially in the HEV environment that includes a variety of interference noises, e.g., Schottky noise, thermal noise and space electromagnetic noise, which may cause random modeling errors thus altering the statistical properties of the system noise. Using regular EKF may result in accumulative errors in the states estimates under the above conditions, and may even cause filter divergence.

This study aims to address the SOC estimation issues using conventional EKF arising from system interference noises in practical applications. A dynamic battery model is first formulated as a basis for SOC estimate. EMF hysteresis is included in the model to improve the SOC estimation. A robust EKF in which the state estimation is decoupled from the bias state estimation is proposed. Using the robust EKF, the state estimation error can be gradually reduced to a minimum under a certain criterion even if the system model contains indeterministic information. Possible sources of modeling bias error are analyzed to enable the tuning of the robust EKF. The effects of the bias vector on state estimation and the acquisition of the bias constant are subsequently addressed. The determination of a near optimum gain coefficient is introduced to decrease the fluctuation of SOC estimation caused by battery terminal voltage fluctuation. The performance of the proposed robust EKF algorithm in SOC estimation of lithium-ion batteries is finally investigated.

2. Modeling of the Lithium-Ion Battery

Modeling of the battery aims to find the relationship between currents and voltages measured at the terminals of the battery. Besides concentration and activation polarization effects lithium ion batteries exhibit an equilibrium potential hysteresis phenomenon. The hysteresis characteristics of the lithium-ion battery have a notable effect on SOC estimation accuracy, and it is therefore important that the model should incorporate these characteristics.

2.1. Hysteresis Characteristics

The cell equilibrium potential depends on its charge and discharge history, and in some batteries exhibits hysteresis. There are many publications on the hysteresis characteristics for nickel-hydrogen batteries; a detailed study is reported in [12,13]. A preliminary study of lithium-ion battery hysteresis characteristics is reported in [14–17]. The hysteresis characteristics of lithium-ion batteries are thought to be due to the intercalation of lithium ions into carbon and $LiMn_2O_4$ electrodes [16], which leads to equilibrium difference between battery charging and discharging. An alternative hypothesis is that the observed hysteresis is due to the slow dynamics of the battery which almost never reaches steady state. Regardless of the source of the observed hysteresis, it needs to be taken into account when estimating the state of charge.

A series of experiments were conducted in order to study the open circuit voltage characteristics of the battery and the influence of the current on its hysteresis during charging and discharging. The lithium-ion battery studied in this paper is composed of 16 cells in series. The battery used had been selected by the manufacturer, and the inconsistency would not affect the model validation. Cell variations were therefore neglected and the battery made up of 16 cells was regarded as a "big cell".

Figure 1(a) shows the open-circuit cell voltage versus SOC under the same charge/discharge current of 30 A. Figure 1(b) shows the open circuit voltage versus SOC for different charge/discharge currents. The testing procedure in Figure 1(a) was as follows: at room temperature, the battery was fully charged, left it in the open-circuit state for 2 hours, and then discharged by 10% of the rated capacity at a current of 30 A. The battery is then kept in the open-circuit state and the open circuit voltage was observed. After 10 hours, the measured battery voltage was regarded to be the equilibrium potential of the battery since its growth rate was negligible. The process was subsequently repeated to get the equilibrium voltage curve during discharge as shown in Figure 1(a). Similarly the battery was charged, and the equilibrium open circuit voltage of the battery was measured every 10% SOC to obtain the open circuit voltage curve during charging. Using the same discharge test procedure described above, the equilibrium potential was also measured when the discharge current was 100 A as shown in Figure 1(b).

From Figure 1(a), it is evident that the equilibrium open circuit voltage of a cell for a given SOC during charge and discharge are different. The OCV measured during charge is higher than that measured during discharge. It is evident in Figure 1(b) that the equilibrium potentials at the discharge current of 30 A and 100 A are nearly the same and the biggest difference is only 3 mV, which means the equilibrium potential of the battery is essentially independent of the battery current, and the difference of equilibrium potential between charge and discharge is an inherent characteristic of the

battery itself. Thus, for a specified open-circuit voltage there are two different SOC values, which introduce uncertainty in SOC determination using the OCV method. Therefore, it is important to analyze the hysteresis characteristics of the battery to reduce SOC estimation error.

Figure 1. Open-circuit cell voltages as a function of SOC at room temperature.
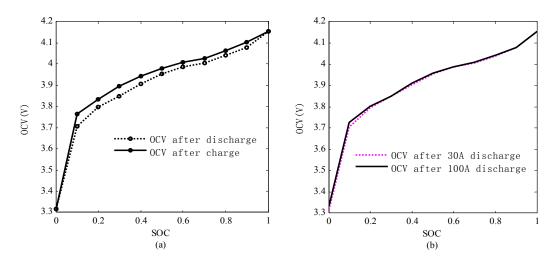

Table 1 shows the equilibrium potential measured during charging process and discharging process when the SOC is 0.5. We find that the OCV after charging is 24 mV higher than that measured after discharging. The difference of 24 mV compared to the whole working voltage range of the battery is small (the voltage range of single battery over the whole SOC working range is around 1200 mV). However, the gradient of the measured OCV of the battery is relatively small in the middle region of SOC and a small hysteresis of 24 mV can cause a significant error in the SOC estimate based on the OCV curve. The practical capacity of the battery used in the experiment is 94 Ah, and the change in capacity per 1 mV change of open-circuit voltage is 0.19 Ah mV-1 in the vicinity of the 50% depth of discharge (DOD). A 24 mV uncertainty in the OCV means a 4.56 Ah capacity estimate uncertainty, with a significant corresponding SOC uncertainty of around 4.85%. It is therefore important that the hysteresis characteristics are included in the battery model used to estimate the SOC.

Table 1. Comparison of the cell OCV during charging and discharging at SOC = 0.5.
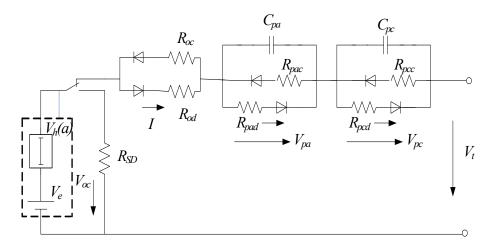
Test conditions	OCV after Charge (V)	OCV after Discharge (V)	Difference (mV)	Average OCV (V)
At room temperature, left at open-circuit state for 10 h	3.979	3.955	24	3.967

2.2. Model Formulation

The proposed equivalent circuit model including OCV hysteresis is shown in Figure 2. It comprises three parts: (1) open-circuit battery voltage V_{oc}, which is composed of an average equilibrium potential V_e and a hysteresis voltage V_h; (2) internal resistance R_i comprising the Ohmic resistance R_o and the polarization resistances, R_{pa} and R_{pc}. R_{pa} represents effective resistance characterizing activation polarization and R_{pc} represents the effective resistance characterizing concentration polarization; (3) effective capacitances C_{pa} and C_{pc}, which are used to describe the activation polarization and

concentration polarization, and used to characterize the transient response of the battery. In addition, ideal diodes are added so that different resistance parameters are used during charging and discharging. The resistances connected in series with the diodes have additional subscripts to indicate charging or discharging. But in the equations these subscripts are omitted for conciseness.

Figure 2. Proposed equivalent circuit model for the lithium-ion battery.

By analyzing the hysteresis characteristics as the function of SOC, the electrical behavior of the circuit can be expressed as follows:

$$\begin{cases} \dot{V}_{pa} = -\dfrac{V_{pa}}{R_{pa}C_{pa}} + \dfrac{I}{C_{pa}} \\[2mm] \dot{V}_{pc} = -\dfrac{V_{pc}}{R_{pc}C_{pc}} + \dfrac{I}{C_{pc}} \\[2mm] \dot{V}_{h} = -\alpha\, sign(I)(V_{h,\max} + sign(I)V_{h}) \\[2mm] V_{t} = V_{e} + V_{h} - V_{pa} - V_{pc} - IR_{o} \end{cases} \tag{1}$$

where *I* is the current through the battery, $V_{h,max}$ represents the maximum hysteresis voltage of the battery as a function of SOC, which is defined as *s*, *α* is hysteresis coefficient, and V_t is the terminal voltage of the battery. In addition, the average open-circuit voltage of the battery is considered as the equilibrium potential V_e in this paper. The extended Kalman filter was used to identify the coupled model parameters reflecting battery polarization characteristics (R_{pa}, C_{pa}, R_{pc}, C_{pc}) and hysterestics (*α*). The parameters characterizing battery equilibrium potential and ohmic resistance were determined experimentally. The identification of the model parameters and dynamic performances were described in detail in the previous papers by the authors [18].

3. SOC Estimation Using Robust Extended Kalman Filtering

3.1. Robust State Estimation

The main idea of robust state estimation is that the modeling errors are regarded as constant bias state vectors. The dynamic states of the system and bias states are estimated separately, and the

dynamic states are subsequently corrected using the bias states estimated values. To get the solution to states and bias estimation of a dynamic system, Friedland proposed decoupling the bias estimation from the state estimation to reduce computational complexity [19]. Hsieh and Chen generalized Friedland's filter and proposed an optimal solution for a two-stage Kalman estimator by applying a two-stage U-V transformation [20,21]. To reduce the number of arithmetic operations in speed and rotor flux estimation of induction machine, Hilairet proposed modified optimal two-stage Kalman estimator derived from Hsieh and Chen algorithm [22]. Considering the nonlinear characteristics of the lithium-ion battery model, we propose in this paper a robust state estimation including EKF, which is suited for nonlinear systems. If modeling errors are neglected, the nonlinear system of interest can be defined by:

$$
\begin{cases}
x_k = f(x_{k-1}, u_{k-1}, w_{k-1}) \\
y_k = h_k(x_k, u_k, v_k) \\
w_k \sim (0, Q_{x,k}) \\
v_k \sim (0, R_k)
\end{cases}
\tag{2}
$$

where x_k is the vector of dynamic states, u_k is the control input, w_k represents process noise which is assumed to be discrete-time Gaussian zero-mean white noise with covariance of $Q_{x,k}$, v_k represents measurement noise which is assumed to be discrete-time Gaussian white noise with zero mean and a covariance of R_k. Taylor series is used to expand the output equation of the nonlinear system at $x_k = \hat{x}_k^-$, the output equation is arranged by [23]:

$$
\begin{aligned}
y_k &= h_k(\hat{x}_k^-, u_k, 0) + \left.\frac{\partial h}{\partial x}\right|_{\hat{x}_k^-} (x_k - \hat{x}_k^-) + \left.\frac{\partial h}{\partial v}\right|_{\hat{x}_k^-} v_k \\
&= h_k(\hat{x}_k^-, u_k, 0) + C_k(x_k - \hat{x}_k^-) + M_k v_k \\
&= C_k x_k + [h_k(\hat{x}_k^-, u_k, 0) - C_k \hat{x}_k^-] + M_k v_k \\
&= C_k x_k + z_k + \tilde{v}_k
\end{aligned}
\tag{3}
$$

where z_k and $\tilde{v}_k$ are defined as follows:

$$
\begin{cases}
z_k = h_k(\hat{x}_k^-, u_k, 0) - C_k \hat{x}_k^- \\
\tilde{v}_k \sim N(0, M_k R_k M_k^T)
\end{cases}
\tag{4}
$$

To allow for modeling errors constant matrices ΔC, ΔA and ΔF are introduced such that the linearized system's equations with modeling error are given by:

$$
x_k = (A_{k-1} + \Delta A)x_{k-1} + (F_{k-1} + \Delta F)u_{k-1} + w_{k-1}
\tag{5}
$$

$$
y_k = (C_k + \Delta C)x_k + z_k + \tilde{v}_k
\tag{6}
$$

where:

$\Delta A = [a_1 \cdots a_n]^T$, $\Delta F = [f_1 \cdots f_n]^T$, $\Delta C = [c_1 \cdots c_n]^T$.

where $a_i \in R^n$, $f_i \in R^q$, $c_i \in R^m$, $i = 1, \cdots, n$.

Define a constant bias vector $b_k \in R^{n(n+q+m)}$ such that $b_k = [a_1^T \cdots a_n^T \quad f_1^T \cdots f_q^T \quad c_1^T \cdots c_m^T]^T$. The Equations (5) and (6) can be rearranged as follows:

$$x_k = A_{k-1}x_{k-1} + F_{k-1}u_{k-1} + B_{k-1}b_{k-1} + w_{k-1} \tag{7}$$

$$y_k = C_k x_k + D_k b_k + z_k + \tilde{v}_k \tag{8}$$

where $B_{k-1} = \begin{bmatrix} x_{k-1}^T & 0 & : & u_{k-1}^T & 0 \\ 0 & x_{k-1}^T & : & 0 & u_{k-1}^T \end{bmatrix}$, $D_k = \begin{bmatrix} 0_m & 0 & : & x_k^T & 0 \\ 0 & 0_m & : & 0 & x_k^T \end{bmatrix}$.

The vector b_k contains the constant bias states, which includes Gaussian white noise in practice, and can be expressed by:

$$b_k = b_{k-1} + \zeta_{k-1} \tag{9}$$

where ζ_k is Gaussian zero-mean white noise, and $E(\xi_i \xi_j^T) = Q_b \delta_{ij}$, $E(w_i \tilde{v}_j^T) = E(w_i \zeta_j^T) = E(\tilde{v}_i \zeta_j^T) = 0$.

The state estimation of the system with modeling error is converted to state estimation of the system with constant bias through the transformation. The robust state estimation combined EKF based on separate bias estimator are derived in detail in appendix A as described in [24]. Combining the equations in appendix A, the estimates of x can be given by:

$$\hat{x}_k^- = A_{k-1}\hat{x}_{k-1}^+ + F_{k-1}u_{k-1} + B_{k-1}\hat{b}_{k-1}^+ \tag{10}$$

$$\tilde{P}_{x,k}^- = A_{k-1}\tilde{P}_{x,k-1}^+ A_{k-1}^T + B_{k-1}Q_{b,k-1}B_{k-1}^T + Q_{x,k-1} \tag{11}$$

$$\tilde{K}_{x,k} = \tilde{P}_{x,k}^- C_k^T (C_k \tilde{P}_{x,k}^- C_k^T + R_k)^{-1} \tag{12}$$

$$\tilde{P}_{x,k}^+ = (I - \tilde{K}_{x,k}C_k)\tilde{P}_{x,k}^- \tag{13}$$

$$K_k = \tilde{K}_{x,k} + V_k K_{b,k} \tag{14}$$

$$\hat{x}_k^+ = \hat{x}_k^- + K_k(y_k - h(\hat{x}_k^-, u_k, 0) - D_k \hat{b}_k^-) \tag{15}$$

From Equations (10) to (15), it is shown that the bias information $B_{k-1}Q_{b,k-1}B_{k-1}^T$ is added to estimate of $\hat{x}$. The vector b_k appears as an input to the system and thus its associated noise Q_b must be included in the estimate of *P*. In Equations (10) to (15), the matrices B_k and D_k contains the states $\hat{x}_{k-1}^+$, which is used instead of the states x_k in this paper:

$$B_k = \begin{bmatrix} \hat{x}_{k-1}^{+T} & 0 & : & u_{k-1}^T & 0 \\ 0 & \hat{x}_{k-1}^{+T} & : & 0 & u_{k-1}^T \end{bmatrix} \quad D_k = \begin{bmatrix} 0_m & 0 & : & \hat{x}_{k-1}^{+T} & 0 \\ 0 & 0_m & : & 0 & \hat{x}_{k-1}^{+T} \end{bmatrix}$$

From the equations, it is inferred that the dynamic states of the system and the bias states are decoupled. They can be estimated based on the proposed robust estimation algorithm, which reduces the dimensions of the dynamic state equations, and further decreases the computation compared to the virtual noise compensation algorithm described in [25].

3.2. SOC Estimation Based on the Proposed Battery Model

SOC can be regarded as a state variable, which is added to the proposed battery model. The discretized system for the equivalent circuit model of the battery can be expressed by [26]:

$$\begin{cases} V_{pa,k} = V_{pa,k-1}\exp(-\Delta t/(R_{pa}C_{pa})) + I_{k-1}R_{pa}(1-\exp(-\Delta t/(R_{pa}C_{pa}))) \\ V_{pc,k} = V_{pc,k-1}\exp(-\Delta t/(R_{pc}C_{pc})) + I_{k-1}R_{pc}(1-\exp(-\Delta t/(R_{pc}C_{pc}))) \\ \quad V_{h,k} = V_{h,k-1}\exp(-\alpha\Delta t) - (1-\exp(-\alpha\Delta t))sign(I)V_{h,\max} \\ \quad\quad s_k = s_{k-1} - \eta_i I_{k-1}\Delta t/C_N \end{cases}$$
$$V_{t,k} = V_e(s_k) - I_k R_o - V_{pa,k} - V_{pc,k} + V_{h,k} \tag{16}$$

where Δt is the sampling interval; s_k represents the SOC, η_i stands for columbic efficiency, which is a function of the battery current. Using curve fitting of the experiment data, the equilibrium potential V_e as the function of SOC was determined as follows:

$$V_e(s_k) = 5.2s_k^4 - 0.86s_k^3 - 12s_k^2 + 15s_k + 59 \tag{17}$$

To estimate the SOC using the Robust EKF, the mathematical model of the battery in (17) needs to be rearranged as:

$$\begin{cases} x_k = A_{k-1}x_{k-1} + F_{k-1}u_{k-1} \\ \quad y_k = h(x_k, u_k) \end{cases} \tag{18}$$

where:

$$x = \begin{bmatrix} V_{pa} & V_{pc} & V_h & s \end{bmatrix}^{\mathrm{T}}, \; u = I, \; y = V_t$$

$$A_{k-1} = \begin{bmatrix} \exp(-\Delta t/(R_{pa}C_{pa})) & 0 & 0 & 0 \\ 0 & \exp(-\Delta t/(R_{pc}C_{pc})) & 0 & 0 \\ 0 & 0 & \exp(-\alpha\Delta t) & 0 \\ 0 & 0 & 0 & 1 \end{bmatrix}$$

$$F_{k-1} = \begin{bmatrix} R_{pa}(1-\exp(-\Delta t/(R_{pa}C_{pa}))) & R_{pc}(1-\exp(-\Delta t/(R_{pc}C_{pc}))) & 0 & \eta_i(I)\Delta t/C_N \end{bmatrix}^{\mathrm{T}}$$
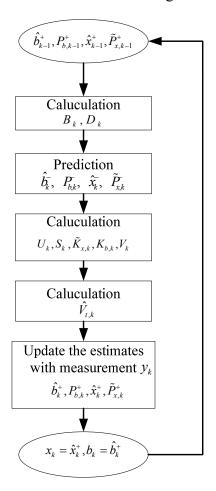
The largest source of error is the SOC estimation error. There are two main possible sources of modeling error. One is the change of the internal resistance caused by the effect of the working environment such as temperature and aging of the battery. The other arises from inaccuracy of the mathematical relationship between the equilibrium potential and SOC since the function is obtained by curve fitting the experiment data; the measurement error and fitting error may lead to estimation error of SOC. Referring to the system Equations (5) and (6) including modeling error, and considering the SOC error components of the battery system, the bias matrix of the battery system can be defined as:

$$\Delta C = \begin{bmatrix} 0 & 0 & 0 & \rho \end{bmatrix}$$

where ρ is a bias constant. The bias vector will be therefore given by:

$$b_k = [0 \quad 0 \quad 0 \quad \rho]^{\mathrm{T}}$$

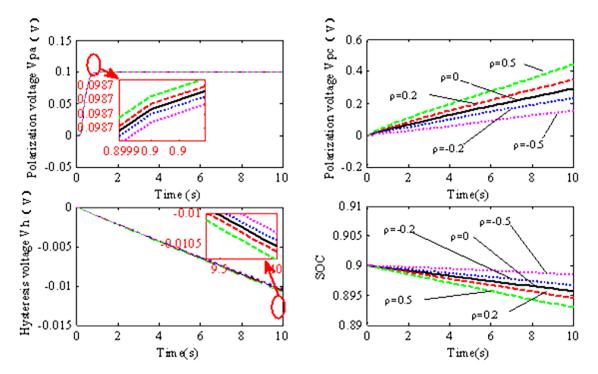The procedure of SOC estimation using the proposed robust EKF algorithm is shown in Figure 3.

Figure 3. Procedure of the Robust EKF algorithm in SOC estimation.

3.3. Analysis of the Effect of the Bias Vector on State Estimation

As described above, the values of the bias vector will have significant effect on robustness of SOC estimation using the Robust EKF algorithm. It is therefore necessary to investigate the influence of the bias constant variation on the estimation of the states of the battery system. Referring to [27], the current of 1C which is at the usual working current range was therefore used as the testing current. The results are shown in Figure 4.

The bias constant ρ as described in Section 3.2 reflects measurement error and coefficient fitting error of the battery system, which impact on the relationship between states (V_{pa}, V_{pc}, V_h and SOC) estimation of the battery dynamics and the parameter ρ is illustrated in Figure 4. From Figure 4, it is seen that the polarization voltage V_{pa} and hysteresis voltage V_h estimate are hardly affected by the variation of the bias constant ρ. But the change in the polarization voltage V_{pc} and SOC estimate for a bias constant value of 0.5 are 0.157 V and 0.01, respectively compared to their value when $\rho = 0$. It is clear that the estimates of V_{pc} and SOC are influenced significantly by the bias constant. The polarization voltage V_{pc} estimate is a monotone increasing function of the variable of bias ρ, which is overestimated when $\rho > 0$ compared and underestimated when $\rho < 0$. In contrast, the SOC estimate is a monotone decreasing function of the variable of bias ρ, which is underestimated when $\rho > 0$, and overestimated when $\rho < 0$.

Figure 4. Impact of bias constant ρ on states estimation.

We therefore conclude that the influence of the bias constant variation on the polarization voltage V_{pa} and hysteresis voltage V_h estimate can be ignored. But the polarization voltage V_{pc} and SOC estimate errors tends to change linearly as the bias constant ρ varying. The value of the bias constant can be determined as discussed in the following section.

3.4. Determining the Bias Constant

Initialization of the covariance matrices expressing disturbance on the plant Q and on the measurement R is an important part of Robust EKF procedure since it impacts significantly on its estimation performance. The dynamic states and bias state are separately estimated in the Robust EKF algorithm. It is therefore necessary to choose the values of the filter parameters for both the dynamic states and bias state parts.

A judicious choice of Q and R is attained from experimental studies under the simplifying assumption that the noise processes $\{w_k\}$ and $\{v_k\}$ are uncorrelated, leading to diagonal Q and R. The initial covariance matrices P_b and Q_b, and the initial weighted matrix were ultimately chosen to be:

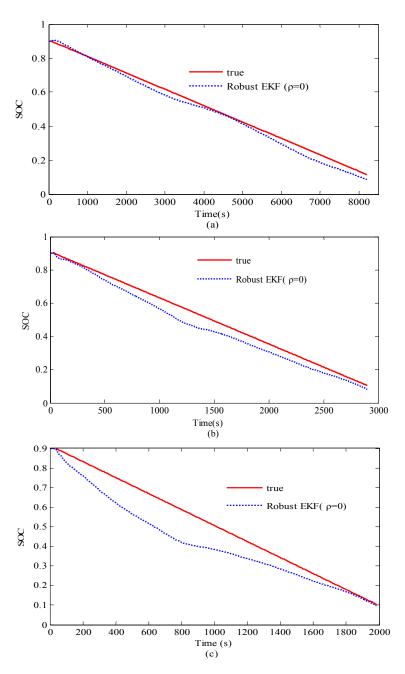$$P_b = 0.01 \,, \; Q_b = 0.00001 \,, \; V = diag(0.001, 0.001, 0.001, 0.001)$$

And the initial covariance matrix $\tilde{P}_x$, together with Q_x and R were given by:

$$Q_x = \begin{bmatrix} 0.0001 & 0 & 0 & 0 \\ 0 & 0.0001 & 0 & 0 \\ 0 & 0 & 0.0001 & 0 \\ 0 & 0 & 0 & 0.0001 \end{bmatrix}, \; \tilde{P}_x = \begin{bmatrix} 10 & 0 & 0 & 0 \\ 0 & 10 & 0 & 0 \\ 0 & 0 & 0.1 & 0 \\ 0 & 0 & 0 & 0.04 \end{bmatrix}, \; R = 5$$
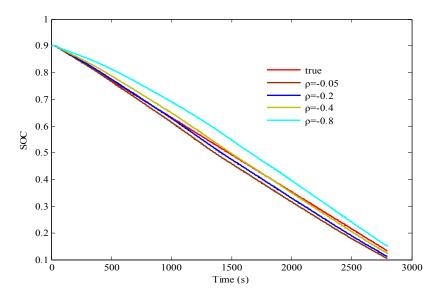
Data obtained from tests of battery discharge at constant current was used in this paper to verify SOC estimation using the proposed battery model with Robust EKF assuming the bias constant ρ is

zero. The measured and estimated SOC of the battery for three rates of discharge of C/3, 1C and 1.5C, respectively, are plotted in Figure 5. From Figures 5(a), (b) and (c), it is clear that the estimated SOC are all less than the true value. The difference between the estimated and measured SOC increases with the battery current. Based on the analysis of the impact of the bias vector on SOC estimation as discussed in Section 3.3, the bias constant ρ needs to be negative to reduce the steady error of SOC estimate. A bias constant ρ ranging from −0.8 to 0 was selected based on the practical results in Figure 6. From Figure 6, it is shown that the SOC estimate is first converging to experimental SOC curve as the bias constant ρ increase, and then is gradually away from true SOC when $\rho > −0.2$. An optimal value of $\rho = −0.4$ is ultimately chosen.

Figure 5. The experimental and estimated SOC of the battery with Robust EKF at $\rho = 0$ ($SOC_0 = 0.9$).

Figure 6. Modified result of Robust EKF estimation with different bias value at the discharge current of 1C ($SOC_0 = 0.9$).

3.5. Tuning of the Filter Gain Coefficient

The greatest advantage of EKF is to make the estimated state with initial error converge quickly to the true value of the state. While the SOC value describing the state of charge of the battery is a gradually changing state variable, the rate of change of the battery terminal voltage is relatively more rapid especially when the current changes direction between charging and discharging, leading to large fluctuations of the terminal voltage error of the battery model, which may further lead to oscillations of the SOC estimate thus enlarging the error. To resolve this problem, an optimal filter gain coefficient r is introduced to adjust the Kalman gain of the SOC in order to improve the stability of SOC estimation while ensuring the required precision. Based on this idea, the states estimation is changed to:
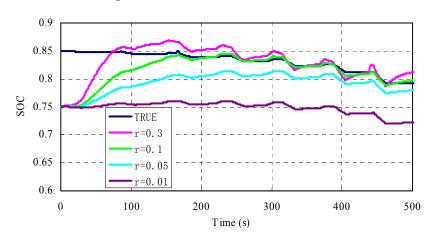
$$\hat{x}_k^+ = \hat{x}_k^- + \Gamma_k K_k (y_k - h(\hat{x}_k^-, u_k, 0) - D_k \hat{b}_k^-)$$ (19)

where $\Gamma_k = \begin{bmatrix} 1 & 0 & 0 & 0 \\ 0 & 1 & 0 & 0 \\ 0 & 0 & 1 & 0 \\ 0 & 0 & 0 & r \end{bmatrix}$.

The value of the gain coefficient *r* directly affects the accuracy and stability of SOC estimation. If the value is too big, the fluctuation of SOC estimate might be enlarged, and the accuracy reduced. If it is too small, filtering convergence speed to the true value of the state may be decreased, and the accuracy of SOC estimation may also be affected.

The convergence speed and estimation accuracy were all taken into consideration during the optimization of the gain coefficient. Based on comparison between experimental and simulation results with different *r* values of ranging from 0.01 to 0.5 were investigated.

In Figure 7, the true SOC value during a hybrid pulse charge/discharge test is compared with the estimated SOC obtained from the Robust EKF algorithm for different gain coefficients assuming the same initial error. It is evident that the bigger the gain coefficient *r*, the faster the convergence speed to the true value of SOC, however, the estimated SOC is easily influenced by the terminal voltage of the
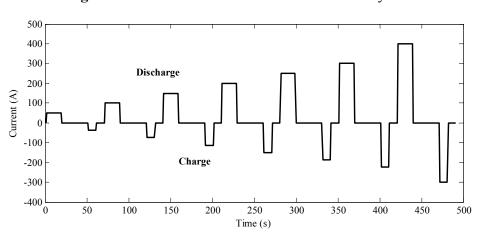
battery. Taking *r* = 0.3 for example, during *t* = 60 s~70 s, the changing from the discharging state to charging state causes the terminal voltage of the battery to rapidly increase, which results in the SOC being over estimated and *vice versa*. When *r* is small, SOC estimation result can reflect the true tendency well, but the speed of convergence to the true value is slow. The trend of the estimated SOC curve is the closest to the "True" plotted in Figure 7 when *r* = 0.01, however, the estimation error may be unacceptably large if the initial error is relatively large. A gain coefficient of 0.1 was ultimately selected to achieve a compromise between the speed of convergence and estimation accuracy.

Figure 7. Effects of various gain coefficient values on SOC estimation with Robust EKF.
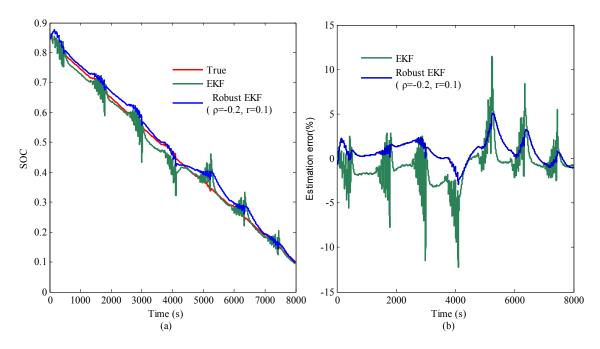

4. Results Discussion

The self-defined hybrid pulse power characterization (self-defined HPPC) shown in Figure 8 was applied for validating SOC estimation using the Robust EKF. Figure 9(a) shows a comparison between the SOC values estimated using both the Robust EKF and regular EKF when the battery SOC decreased from 0.9 to 0.1 at the self-defined HPPC cycles. The estimation error is shown in Figure 9(b). From Figure 9 we find that using regular EKF, the SOC estimation changes with the voltage fluctuations rapidly, and the maximum estimation error can be over 10%, which does not satisfy the requirement of electric vehicle. Using the proposed Robust EKF algorithm, the estimation error is within 5% during the entire process of charging and discharging of the battery, thus meeting the SOC accuracy requirement.
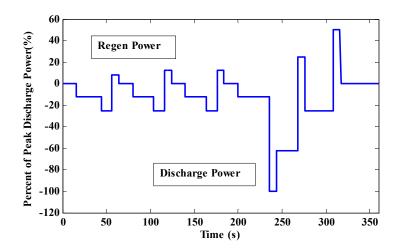
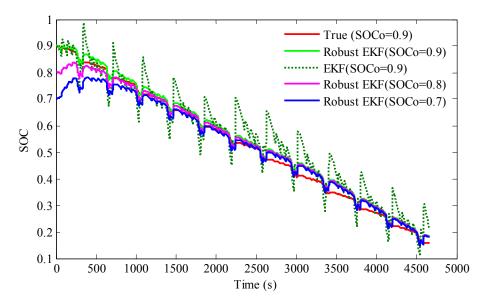**Figure 8.** Profile of self-defined HPPC for one cycle.

Figure 9. Comparing results of SOC estimation with the proposed Robust EKF and EKF for self-defined HPPC cycles.

(a) (b)

The DST driving cycles was also used to validate the SOC estimation performance using Robust EKF algorithm. One cycle DST profile is illustrated in Figure 10. The measured SOC and the estimated SOC for different SOC initial values are illustrated in Figure 11 (the true initial SOC value was 0.9). It is seen that the estimated SOC using the Robust EKF converges faster to the measured SOC values, and the estimation accuracy is significantly improved compared to SOC estimate using EKF only. When the initial SOC values are set to 0.8 and 0.7, the SOC estimation error with Robust EKF falls to within 6% of the true value after 300 s and 600 s' correction, respectively. Furthermore, the SOC estimation error using the Robust EKF is enlarged when the SOC is in the range from 0.55 to 0.2. This is because the battery terminal voltage reduces and the output current supplied by the battery increase (for given power output) with the passage of time, which results in serious polarization of the battery, leading to large estimation error. The SOC estimation error using Robust EKF is controlled within 5% during the entire DST driving cycles.

Figure 10. DST power profile for one cycle.

Figure 11. Estimated and tested SOC for DST driving cycles (SOC$_0$ = 0.9).

5. Conclusions

The paper presented an equivalent circuit model with two RC networks characterizing battery activation and concentration polarization processes. It is noticeable that cell variations need to be taken into account in battery pack simulation. The battery pack consistency evaluation system including cell SOC, ohmic resistance, polarization voltage and maximum available capacity variations will be introduced in the battery module simulation, which will be the key research point in the future work. The hysteresis voltage was also included in the battery model to improve the accuracy of SOC determination. The paper proposed a Robust Extended Kalman filter in which the steady error of the SOC estimation was investigated, and accounted for to improve the estimation accuracy. Based on the knowledge of battery characteristics, a filter gain coefficient was introduced to decrease the fluctuation of SOC estimation caused by terminal voltage fluctuation, which occurs when a standard EKF is used without the gain coefficient. Simulation results demonstrated the accuracy of SOC estimation with the proposed Robust EKF during both the self-defined HPPC cycles and DST driving cycles. The error found to be less than 5% compared to nearly 10% error achieved by the standard EKF.

Acknowledgments

Appendix A

The robust state estimation combined EKF based on separate bias estimator can be derived as follows. In the absence of bias error the vector b_k is zero, the estimates of x using EKF are given by:

$$\tilde{x}_k^- = A_{k-1}\tilde{x}_{k-1}^+ + F_{k-1}u_{k-1} \qquad (A.1)$$

$$\tilde{P}_{x,k}^- = A_{k-1}P_{x,k-1}^+ A_{k-1}^T + Q_{x,k-1} \qquad (A.2)$$

$$\tilde{P}^+_{x,k} = (I - \tilde{K}_{x,k} C_k) \tilde{P}^-_{x,k} \qquad (A.3)$$

$$\tilde{x}^+_k = \tilde{x}^-_k + \tilde{K}_{x,k}(y_k - h(\tilde{x}^-_k, u_k, 0)) \qquad (A.4)$$

with initial condition $\tilde{P}_x(0) = P_x(0)$. $\tilde{x}$ is the bias-free estimate of x, $\tilde{P}_x$ is the error covariance matrix of $\tilde{x}$, $\tilde{K}_x$ is the Kalman gain matrix, Q_x is the process noise covariance matrix of $\tilde{x}$, R is the measurement noise covariance matrix.

The bias vector estimator is given by:

$$\hat{b}^-_k = \hat{b}^+_{k-1} \qquad (A.5)$$

$$P^-_{b,k} = P^+_{b,k-1} + Q_{b,k-1} \qquad (A.6)$$

$$K_{b,k} = P^-_{b,k} S^T_k (S_k P^-_{b,k} S^T_k + C_k P^-_{x,k} C^T_k + R_k)^{-1} \qquad (A.7)$$

$$P^+_{b,k} = (I - K_{b,k} S_k) P^-_{b,k} \qquad (A.8)$$

$$\hat{b}^+_k = \hat{b}^-_k + K_{b,k}[y_k - h(\hat{x}^-_k, u_k, 0) - D_k \hat{b}^-_k] \qquad (A.9)$$

where the weighted matrices U, S, and V are defined by:

$$U_k = A_k V_{k-1} + B_k \qquad (A.10)$$

$$S_k = C_k U_k + D_k \qquad (A.11)$$

$$V_k = U_k - \tilde{K}_{x,k} S_k \qquad (A.12)$$

Considering the estimates of $\tilde{x}$ and $\hat{b}$, the adjusted estimates of x are defined by:

$$\hat{x}^-_k = \tilde{x}^-_k + U_k \hat{b}^-_k \qquad (A.13)$$

$$\hat{x}^+_k = \tilde{x}^+_k + V_k \hat{b}^+_k \qquad (A.14)$$

where the present estimate $\tilde{x}$ is adjusted with the current estimate of the bias vector $\hat{b}$.

References

1. Piller, S.; Perrin, M.; Jossen, A. Methods for state-of-charge determination and their applications. *J. Power Sources* **2001**, *96*, 113–120.
2. Sato, S.; Kawamura, A. A New Estimation Method of State of Charge using Terminal Voltage and Internal Resistance for Lead Acid Battery. In *Proceedings of 2002 IEEE International Conference on Power Conversion*, Osaka, Japan, 2–5 April 2002.
3. Soon, Ng.K.; Moo, C.S.; Chen, Y.P.; Hsieh, Y.C. Enhanced coulomb counting method for estimating stat-of-charge and state-of-health of lithium-ion batteries. *Appl. Energy* **2009**, *86*, 1506–1511.
4. Piller, S.; Perrin, M.; Jossen, A. Methods for state-of-charge determination and their applications. *J. Power Sources* **2001**, *96*, 113–120.
5. Shen, W.X. State of available capacity estimation for lead-acid batteries in electric vehicles using neural network. *Energy Convers. Manag.* **2007**, *48*, 433–442.

6. Cai, C.; Du, D.; Liu, Z.; Ge, J. State-of-charge (SOC) Estimation of High Power Ni-MH Rechargeable Battery with Artificial Neural Network. In *Proceedings of 9th IEEE International Conference on Neural Information*, Singapore, 18–22 November 2002.

7. Grewal, M.S.; Andrews, A.P. *Kalman Filtering, Theory and Practice*; Prentice Hall: Upper Saddle River, NJ, USA, 1993.

8. Plett, G.L. Extended Kalman filtering for battery management systems of LiPB-based HEV battery packs—Part 3: State and parameter estimation. *J. Power Sources* **2004**, *134*, 277–292.

9. Vasebi, A.; Bathaee, S.M.T.; Partovibakhsh, M. Predicting state of charge of lead-acid batteries for hybrid electric vehicles by extended Kalman filter. *Energy Convers. Manag.* **2008**, *49*, 75–82.

10. Han, J.; Kim, D.; Sunwoo, M. State-of-charge estimation of lead-acid batteries using an adaptive extended Kalman filtering. *J. Power Sources* **2009**, *188*, 606–612.

11. He, H.W.; Xiong, R.; Fan, J.X. Evaluation of lithium-ion battery equivalent circuit models for state of charge estimation by an experimental approach. *Energies* **2011**, *4*, 582–598.

12. Ta, K.P.; Newman, J. Proton intercalation hysteresis in charging and discharging nickel hydroxide electrodes. *J. Electrochem. Soc.* **1999**, *146*, 2769–2779.

13. Srinivasan, V.; Weidner, J.W.; Newman, J. Hysteresis during cycling of nickel hydroxide active material. *J. Electrochem. Soc.* **2001**, *148*, A969–A980.

14. Murray, J.J.; Sleigh, A.K.; Mckinnon, W.R. Heats and hysteresis in calorimetry of Li/Li_xMnO_2 cells. *Electrochim. Acta* **1991**, *36*, 489–498.

15. Sleigh, A.K.; Murray, J.J.; Mckinnon, W.R. Memory effects due to phase conversion and hysteresis in Li/Li_xMnO_2 cells. *Electrochim. Acta* **1991**, *36*, 1469–1474.

16. Zheng, T.; McKinnon, W.R.; Dahn, J.R. Hysteresis during lithium insertion in hydrogen-containing carbons. *J. Electrochem. Soc.* **1996**, *143*, 2137–2145.

17. Inaba, M.; Fujikawa, M.; Abe, T.; Ogumi, Z. Calorimetric study on the hysteresis in the charge-discharge profiles of mesocarbon microbeads heat-treated at low temperatures. *J. Electrochem. Soc.* **2000**, *147*, 4008–4012.

18. Zhang, C.P.; Zhang, C.N.; Liu, J.Z.; Sharkh, S.M. Identification of dynamic model parameters for lithium-ion batteries used in hybrid electric vehicles. *High Technol. Lett.* **2010**, *16*, 6–12.

19. Friedland, B. Treatment of bias in recursive filtering. *IEEE Trans. Autom. Control* **1969**, *AC-14*, 359–367.

20. Hsieh, C.S.; Chen, F.C. Optimal solution of the two-stage Kalman estimator. *IEEE Trans. Autom. Control* **1999**, *44*, 194–199.

21. Chen, F.C.; Hsieh, C.S. Optimal multistage Kalman estimators. *IEEE Trans. Autom. Control* **2000**, *45*, 2182–2188.

22. Hilairet, M.; Auger, F.; Berthelot, E. Speed and rotor flux estimation of induction machine using a two-stage extended Kalman filter. *Automatica* **2009**, *45*, 1819–1827.

23. Simon, D. *Optimal State Estimation: Kalman, H Infinity, and Nonlinear Approaches*; John Wiley &Sons: Hoboken, NJ, USA, 2006.

24. Ignagni, M.B. Separate-bias Kalman estimator with bias state noise. *IEEE Trans. Autom. Control.* **1990**, *35*, 338–341.

25. Deng, Z. *Self-Tuning Filtering Theory with Applications: Modern Time Series Analysis Method*; Harbin Institute of Technology Press: Harbin, China, 2003.

26. Frankin, G.F.; Powell, J.D.; Workman, M.L. *Digital Control of Dynamic Systems*; Addison-Wesley: Boston, MA, USA, 1998.

27. Lu, X.J.; Lin, C.T.; Chen, Q.S.; Han, X. Comparison study of 3 types of battery models for electrical vehicle. *Chin. J. Power Sources* **2006**, *130*, 535–538.